THERMAL RADIATION EFFECTS ON THE ONSET OF UNSTEADINESS OF FLUID FLOW IN VERTICAL MICROCHANNEL FILLED WITH HIGHLY ABSORBING MEDIUM

by

M. Y. ABDOLLAHZADEH JAMALABADI[a,b]***, Jae Hyun PARK***[c*]***,***
and Chang Yeop LEE[d]

[a] Maritime University of Chabahar, Chabahar, Iran
[b] Graduate School of Mechanical and Aerospace Engineering, Gyeongsang National University, Jinju, Gyeongnam, South Korea
[c] Department of Aerospace and System Engineering and Research Center for Aircraft Parts Technology, Gyeongsang National University, Jinju, Gyeongnam, South Korea
[d] Thermochemical Energy System R&BD Group, Korea Institute of Industrial Technology, Cheonan, South Korea

Original scientific paper
DOI:10.2298/TSCI140418124A

This study presents the effect of thermal radiation on the steady flow in a vertical micro channel filled with highly absorbing medium. The governing equations (mass, momentum, and energy equation with Rosseland approximation and slip boundary condition) are solved analytically. The effects of thermal radiation parameter, the temperature parameter, Reynolds number, Grashof number, velocity slip length, and temperature jump on the velocity and temperature profiles, Nusselt number, and skin friction coefficient are investigated. Results show that the skin friction and the Nusselt number are increased with increase in Grashof number, velocity slip, and pressure gradient while temperature jump and Reynolds number have an adverse effect on them. Furthermore, a criterion for the flow unsteadiness based on the temperature parameter, thermal radiation parameter, and the temperature jump is presented.

Key words: *thermal radiation; rarefaction effects, mixed convection, micro channel, flow unsteadinesss*

Introduction

Heat transfer in free and mixed convection in vertical channels is found in many applications [1-4] such cooling systems for electronic devices [5], chemical processing equipment [6], microelectronic cooling [7], *etc*. Solar thermal collector, which absorbs sunlight and convert to heat, is a typical example utilizing such configuration [8, 9]. Different from the other applications [10-13], in the solar collector the radiative heat transfer is significant in addition to conduction and convection. Also, the significance of radiative heat transfer is found in the industrial processes and MHD flow [14-18]. The radiative heat transfer is common. Recently, the use of microchannel in solar collector has been increasing because the miniaturized devices produce higher performance [19-21]. Even though many researchers have performed the steady-state analysis of solar collector considering combined heat transfer of conduction,

* Corresponding author; e-mail: parkj@gnu.ac.kr

convection, and radiation and fluid flow, the onset of flow unsteadiness has been hardly paid attention to. Upon the unsteadiness of the system, many aspects in numerical analysis could be changed; therefore the identification of limit of flow unsteadiness is essential to choose an efficient computational method [22].

When fluid flow is confined by small system such as micro/nano-channels, some discontinuity in velocity and temperature profiles might happen at the interface of fluid and solid surface [23, 24]. Ulmanella and Ho [23] experimentally observed the velocity for various micro-sized channels, which is a function of shear rate, type of liquid and surface morphology. Bocquet and Barrat [24] describe a possibility of temperature jump along with velocity slip. The velocity slip and temperature jump relations should be used as the boundary conditions for liquid-solid interface of micro/nano-sized channel [25].

The purpose of solar thermal collector is to absorb the sunlight as much as possible and a number of studies have been focused to increase the absorptivity of the fluid medium in the solar collector. Recently, the researchers have found that the absorptivity can be significantly enhanced by using nanofluid that is a mixture of liquid and the nanoparticles suspended [19]. With seeding the nanoparticle in base fluid, the extinction coefficient of the medium increases over 100 cm^{-1} [19]. It is apparently optically thick medium even for the microchannel whose characteristic length is in microscale and therefore the optically thick medium approximation is applicable to the analysis of radiative transfer.

Considering all the above-mentioned, in this study we theoretically investigate the thermal radiation effects on the onset of unsteadiness of fluid flow in vertical microchannel filled with highly absorbing medium. This kind of configuration is commonly found in thermal storage with solar collector [17] and thermo-syphon solar water heaters [18]. The velocity slip and temperature jump are modeled by introducing velocity slip length and temperature slip length, respectively. The radiative heat transfer through the medium is simplified by the diffusion approximation (or, Rosseland approximation). Besides the thermal radiation and rarefaction effects, the flow characteristics are identified by using the classical thermo-fluid parameters such as Reynolds number, Grashof number, Nusselt number, and skin friction coefficient are also focused. Finally, the influence of thermal radiation and rarefaction effects on the flow unsteadiness is examined.

Governing equations and numerical method

In order to understand the fundamental basics of an infinitely long vertical solar collector in micro-scale, we considered a simple configuration as shown in fig. 1. An optically thick incompressible fluid is confined by two parallel planar walls that are separated by the distance of $2L$. Since we assume the infinitely long geometry, the flow velocity u is only the function of y-direction across the channel and the origin of the system is placed at the middle point. The left and right walls ($y = \pm L$) are maintained at the uniform temperatures of T_L and T_R, respectively. In the steady-state, this system can be described by momentum and energy equations employing Boussinesq approximation for buoyancy force:

– momentum equation

$$\frac{\partial^2 u}{\partial y^2} = \frac{1}{\mu}\frac{\mathrm{d}p}{\mathrm{d}x} - \frac{\rho_0}{\mu} g\beta\left(T - T_{ref}\right) \tag{1}$$

– energy equation [26]

$$\frac{\partial^2 T}{\partial y^2} = -\frac{4\sigma}{3k\chi}\frac{\partial^2 T^4}{\partial y^2} \tag{2}$$

where dp/dx is a pressure gradient in the flow direction, *i. e.* x-direction, which is perpendicular to the y-direction, T is the medium temperature, k is the thermal conductivity of the fluid, β is the thermal expansion coefficient, μ is the dynamic viscosity, ρ is the fluid density, and T_{ref} is a constant reference temperature defined as $T_{ref} = (T_L + T_R)/2$. The σ is the Stefan-Boltzmann constant and χ is the mean absorption coefficient of the medium. Since the channel size is in micro-scale, the velocity slip and the temperature jump need to be considered as the boundary conditions at the solid walls:

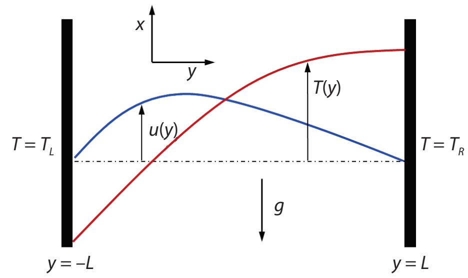

Figure 1. Schematic of the the system

$$u(y=L)=l_v\left(\frac{\mathrm{d}u}{\mathrm{d}y}\right)_{y=L} \tag{3}$$

$$u(y=-L)=l_v\left(\frac{\mathrm{d}u}{\mathrm{d}y}\right)_{y=-L} \tag{4}$$

$$T(y=L)=T_R+l_T\left(\frac{\mathrm{d}T}{\mathrm{d}y}+\frac{4\sigma}{3k\chi}\frac{\partial T^4}{\partial y}\right)_{y=L} \tag{5}$$

$$T(y=-L)=T_R+l_T\left(\frac{\mathrm{d}T}{\mathrm{d}y}+\frac{4\sigma}{3k\chi}\frac{\partial T^4}{\partial y}\right)_{y=-L} \tag{6}$$

where l_v is the velocity slip length and l_T is the characteristic length of temperature jump, which is referred to as "temperature jump length" hereafter. The modelling of velocity slip and temperature jump at fluid-solid interface is not easy due to the complexity of the phenomena themselves. However, in this study we have used the simplest models of eqs. (3)-(6), which resemble those for gas-solid interface, because our purpose is to investigate the physical essence rather than the quantitative details. Nevertheless, we can still obtain the correct physical essence from the simplest velocity slip and temperature jump models even though they could have clear limitation in predicting the accurate quantities.

In order to clarify the physical essence, in this study the following non-dimensionalized variables are introduced:

$$X=\frac{x}{L} \tag{7}$$

$$Y=\frac{y}{L} \tag{8}$$

$$U(Y)=\frac{u(y)}{u_m} \tag{9}$$

$$\theta(Y)=\frac{2T-T_L-T_R}{T_R-T_L} \tag{10}$$

$$P = \frac{pL}{\mu u_m} \tag{11}$$

$$\mathrm{Gr} = \frac{g\beta\left(T_R - T_L\right)L^3}{2\nu^2} \tag{12}$$

$$\mathrm{Re} = \frac{u_m L}{\nu} \tag{13}$$

$$R_d = \frac{\sigma\left(T_R - T_L\right)^3}{6k\chi} \tag{14}$$

$$\theta_R = \frac{T_R + T_L}{T_R - T_L} \tag{15}$$

$$\lambda_v = \frac{l_v}{L} \tag{16}$$

$$\lambda_T = \frac{l_T}{L} \tag{17}$$

where the

$$u_m = \frac{1}{2}\int_{-L}^{L} u\left(y\right)\mathrm{d}y$$

is a constant, Gr is the Grashof number, Re is the Reynolds number, R_d is the radiation parameter, and θ_R is the temperature parameter. Then, the momentum and energy eqs. (1) and (2) can be rewritten as:

$$\frac{\mathrm{d}^2U}{\mathrm{d}Y^2} = -\frac{\mathrm{Gr}\theta}{\mathrm{Re}} + \frac{\mathrm{d}P}{\mathrm{d}X} \tag{18}$$

$$\frac{\mathrm{d}^2}{\mathrm{d}Y^2}\left[\theta + R_d(\theta + \theta_R)^4\right] = 0 \tag{19}$$

$$U\left(Y = 1\right) = \lambda_v\left(\frac{\mathrm{d}U}{\mathrm{d}Y}\right)_{Y=1} \tag{20}$$

$$U\left(Y = -1\right) = \lambda_v\left(\frac{\mathrm{d}U}{\mathrm{d}Y}\right)_{Y=-1} \tag{21}$$

$$\theta\left(Y = 1\right) = 1 + \lambda_T\frac{\mathrm{d}}{\mathrm{d}Y}\left[\theta + R_d(\theta + \theta_R)^4\right]_{Y=1} \tag{22}$$

$$\theta\left(Y = -1\right) = -1 + \lambda_T\frac{\mathrm{d}}{\mathrm{d}Y}\left[\theta + R_d(\theta + \theta_R)^4\right]_{Y=-1} \tag{23}$$

where eqs. from (20) to (23) are the boundary conditions. Also, the skin friction drag coefficient and the Nusselt number are expressed as:

$$C_f\Big|_{y=L} = \frac{\left(\dfrac{\mathrm{d}U}{\mathrm{d}Y}\right)_{Y=1}}{\mathrm{Re}} \tag{24}$$

$$C_f\Big|_{y=-L} = \frac{\left(\dfrac{\mathrm{d}U}{\mathrm{d}Y}\right)_{Y=-1}}{\mathrm{Re}} \tag{25}$$

$$\mathrm{Nu}\Big|_{y=L} = \frac{4\left(\dfrac{\mathrm{d}\left[\theta + R_d\left(\theta+\theta_R\right)^4\right]}{\mathrm{d}Y}\right)_{Y=1}}{\int\limits_{-1}^{1} U\left[\theta - \theta\left(Y=1\right)\right]\mathrm{d}Y} \tag{26}$$

$$\mathrm{Nu}\Big|_{y=-L} = \frac{4\left(\dfrac{\mathrm{d}\left[\theta + R_d(\theta+\theta_R)^4\right]}{\mathrm{d}Y}\right)_{Y=-1}}{\int\limits_{-1}^{1} U(\theta - \theta(Y=-1))\mathrm{d}Y} \tag{27}$$

Results and discussion

In the simplest condition in which rarefaction effects and the thermal radiation are not included ($\lambda_v = \lambda_t = R_d = 0$), the eqs. (18-23) have the following analytical solutions:

$$\theta = Y \tag{28}$$

$$U = \left(\frac{\mathrm{Gr}}{6\,\mathrm{Re}}Y + \frac{3}{2}\right)\left(1 - Y^2\right) \tag{29}$$

$$\mathrm{d}P/\mathrm{d}X = -3 \tag{30}$$

In fig. 2(a), the velocity profiles are plotted by changing Gr/Re from 0 to 54 by the increment of 9. Since the Grashof number, is the ratio of buoyancy to viscous force and the Reynolds number, is the ratio of momentum to viscous forces, the Gr/Re represents the dominance of buoyancy over momentum. When Gr/Re < 9, the velocity profile has a parabolic shape with a single maximum of 3/2 near the origin. Then, with further increase in Gr/Re, two local extrema are observed at:

$$Y = -\frac{3\,\mathrm{Re}}{\mathrm{Gr}} - \sqrt{\left(\frac{3\,\mathrm{Re}}{\mathrm{Gr}}\right)^2 + \frac{1}{3}} \quad \text{(local minimum)},$$

and

$$Y = -\frac{3\,\mathrm{Re}}{\mathrm{Gr}} + \sqrt{\left(\frac{3\,\mathrm{Re}}{\mathrm{Gr}}\right)^2 + \frac{1}{3}} \quad \text{(local maximum)}.$$

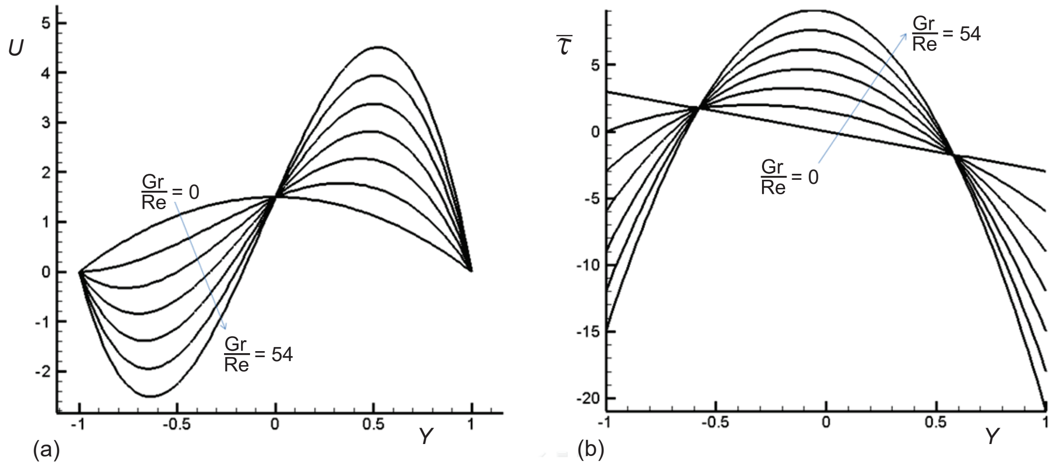

Figure 2. The effect of the ratio of Grashof number to Reynolds number (Gr/Re) on (a) velocity and (b) shear stress without rarefaction effects and thermal radiation ($\lambda_v = \lambda_t$ = Rd = 0)

Figure 2(b) shows the dimensionless shear stress profiles without rarefaction effects and thermal radiation. Following fig. 2(a), Gr/Re varies from 0 to 54 by the increment of 9. The dimensionless shear stress is defined as $\overline{\tau} = \tau / \mu u_m$. The maximum shear stress is observed:

$$\tau_{\max} = \frac{\mu u_m}{L}\left(\frac{4.5\,\mathrm{Re}}{\mathrm{Gr}} + \frac{\mathrm{Gr}}{6\,\mathrm{Re}}\right) \quad \text{at} \quad Y = -\frac{3\,\mathrm{Re}}{\mathrm{Gr}}$$

The skin friction coefficient at the right and left walls are different as:

$$C_f\Big|_{y=\pm L} = -\frac{\mathrm{Gr}}{2\,\mathrm{Re}^2} \mp \frac{3}{\mathrm{Re}}$$

due to the presence of the pressure gradient. The relation of C_f indicates that the natural convection augments the flow in the hot wall side and increases the wall skin fraction while it reduces the flow in the cold wall side and decreases the wall skin fraction.

Without the thermal radiation, Nusselt number at the wall can be expressed:

$$\mathrm{Nu}\Big|_{y=\pm L} = \frac{\mathrm{Re}}{\mathrm{Gr}/90 \mp 0.5\,\mathrm{Re}}$$

When the Grashof number equals to 45 times of Reynolds number, the average temperature is the same as right wall temperature and the Nusselt number at the right wall becomes infinity.

Figure 3 show the effect of radiation parameter, R_d, and temperature parameter, θ_R on the temperature and the velocity profiles without including rarefaction effects ($\lambda_v = \lambda_l = 0$). The ratio of Grashof number to Reynolds number is fixed at 54. Without radiation effect, the temperature profile is linear. However, with the increase in R_d the medium temperature increases in overall while it has a sudden drop near the left cold wall. Such drop is also observed with the reduced temperature parameter, θ_R. The effect of R_d is saturated for $R_d > 10$. The profile with $R_d = 10$ is not much different from the curve with $R_d = 1000$. Different from the temperature, the velocity profile is remarkably changed with R_d. When $R_d = 0$, the velocity in the right side is

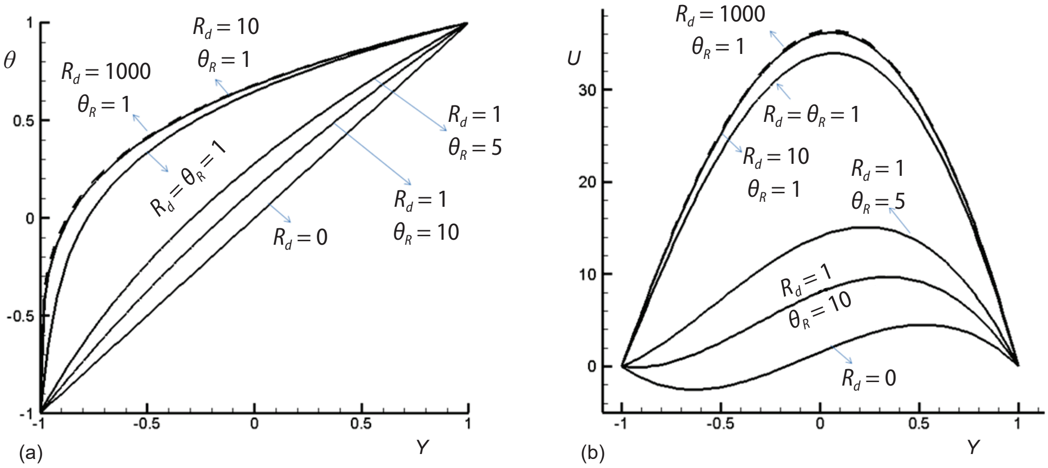

Figure 3. Effect of radiation parameter, R_d, and temperature parameter, θ_R, on (a) temperature and (b) velocity without rarefaction effects ($\lambda_v = \lambda_t = 0$, Gr/Re = 54)

observed larger than the value in the left side (sinusoidal form). However, with the increase in R_d the profile converted to a parabolic shape along with a significant increase of the maximum value. Such behavior is also observed with reduced θ_R.

Next, we consider the case in which the rarefaction effects are included while the thermal radiation is still ignored ($R_d = 0$). In this case, the temperature and velocity profiles are obtained:

$$\theta = Y + \lambda_T \tag{31}$$

$$U(Y) = \left(\frac{-\mathrm{Gr}}{6\,\mathrm{Re}}Y + \frac{\mathrm{d}P}{2\mathrm{d}X} - \frac{\lambda_T \mathrm{Gr}}{2\,\mathrm{Re}}\right)\left(Y^2 - 1\right) + \lambda_v\left(\frac{\mathrm{d}P}{\mathrm{d}X} - \frac{\lambda_T \mathrm{Gr}}{\mathrm{Re}}\right)\left(Y + \lambda_v\right) - \frac{\lambda_v \mathrm{Gr}}{3\,\mathrm{Re}} \tag{32}$$

$$\frac{\mathrm{d}P}{\mathrm{d}X} = \lambda_T \frac{\mathrm{Gr}}{\mathrm{Re}} + \frac{\dfrac{\lambda_v \mathrm{Gr}}{3\,\mathrm{Re}} + 1}{\lambda_v^{\,2} - \dfrac{1}{3}} \tag{33}$$

The effect of temperature jump appears only in the temperature as increase the profile by λ_T, *i. e*. It does not affect the fluid velocity. Figure 4 compares the velocity profiles by changing λ_v while Gr/Re is fixed at 54. The velocity profile is significantly influenced by the slip length: when $\lambda_v < 1/(3^{1/2})$, the increase in λ_v causes the increase in the velocity, while when $\lambda_v \geq 1/(3^{1/2})$, the increase in λ_v causes the decrease in the velocity. The maximum velocity is found either at the wall or at the following position:

$$Y = \frac{\dfrac{\mathrm{Re}}{\mathrm{Gr}} + \dfrac{\lambda_v}{3} \mp \sqrt{\lambda_v^{\,4} + \dfrac{2\lambda_v^{\,3}\,\mathrm{Re}}{\mathrm{Gr}} - \dfrac{\lambda_v^{\,2}}{3} + \left(\dfrac{\mathrm{Re}}{\mathrm{Gr}}\right)^2 + \dfrac{1}{27}}}{\lambda_v^{\,2} - \dfrac{1}{3}} \tag{34}$$

where the tangent of velocity is zero. The velocities at the left and right walls given:

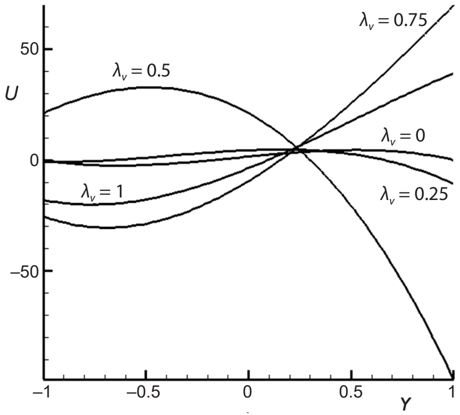

Figure 4. The effect of slip length, λ_v, on the velocity profile without thermal radiation (R_d = 0, Gr/Re = 54)

$$U(\pm 1) = \lambda_v \left(\frac{\mathrm{d}P}{\mathrm{d}X} - \frac{\lambda_T \mathrm{Gr}}{\mathrm{Re}} \right)(\pm 1 + \lambda_v) - \frac{\lambda_v \mathrm{Gr}}{3\,\mathrm{Re}} \tag{35}$$

From the dimensionless pressure gradient relation of eq. (33), we obtain the following relation:

$$\frac{\mathrm{d}p}{\mathrm{d}x} = \lambda_T \rho g \beta (T_R - T_L) + \frac{\frac{\lambda_v}{6} \rho g \beta (T_R - T_L) + \frac{\mu u_m}{L^2}}{\lambda_v^2 - \frac{1}{3}} \tag{36}$$

It indicates that for a given flow rate, the pressure gradient increases with larger velocity slip and temperature jump. The gradient is also augmented as Gr/Re increases. Finally, the skin friction coefficient and the Nusselt number can be derived as:

$$C_f \big|_{y=\pm L} = -\frac{\mathrm{Gr}}{2\,\mathrm{Re}^2} - \frac{\mp \frac{\lambda_v \mathrm{Gr}}{3\,\mathrm{Re}} \mp 1 + \frac{\lambda_v^2 \mathrm{Gr}}{2\,\mathrm{Re}} + \frac{\mathrm{Gr}}{18\,\mathrm{Re}} - \lambda_v}{\mathrm{Re}\left(\lambda_v^2 - \frac{1}{3} \right)} \tag{37}$$

$$\mathrm{Nu}\big|_{y=\pm L} = \left[\frac{\frac{\mathrm{Gr}}{54\,\mathrm{Re}} - \frac{\lambda_v}{6}}{\lambda_v^2 - \frac{1}{3}} + \frac{\mathrm{Gr}}{15\,\mathrm{Re}} \mp 0.5 \right]^{-1} \tag{38}$$

With increase in Gr/Re and velocity slip, both skin friction coefficient and Nusselt number increase. It is noteworthy that the temperature jump has no effect on the skin friction coefficient and the Nusselt number.

Without velocity slip and temperature jump ($\lambda_v = \lambda_T = 0$), from eqs. (18-23), we can derive an implicit formula for the temperature as:

$$\theta + R_d (\theta + \theta_R)^4 = \left[1 + 4R_d \left(\theta_R^3 + \theta_R \right) \right] Y + R_d \left(\theta_R^4 + 6\theta_R^2 + 1 \right) \tag{39}$$

If the optical thickness of medium is remarkably large ($\chi >> 1$) and subsequently $R_d << 1$, from the perturbation method in the first order ($\theta = Y + \theta_0 R_d$) the above equation can be simplified as:

$$R_d \theta_0'' + 4R_d^2 \theta_0'' (Y + R_d \theta_0 + \theta_R)^3 + 12 R_d (1 + R_d \theta_0')^2 (Y + R_d \theta_0 + \theta_R)^2 = 0 \tag{40}$$

The first-order approximation of eq. (40) appears as:

$$\theta_0'' = -12(Y + \theta_R)^2 \tag{41}$$

with subject to the boundary conditions of:

$$\theta_0(-1)=0 \tag{42}$$

$$\theta_0(1)=0 \tag{43}$$

Then, the first-order solution can be obtained:

$$\theta = Y + R_d\left(\frac{(1+\theta_R)^4-(1-\theta_R)^4}{2}Y+\frac{(1+\theta_R)^4+(1-\theta_R)^4}{2}-\left(Y+\theta_R\right)^4\right) \tag{44}$$

Equation (39) has a minimum as $\theta=-(4R_d)^{-1/3}-\theta_R$, which is unconditionally greater than zero. Therefore, the eqs. (39) and (44) always have the real solutions. Figure 5 compares $\theta-\theta(R_d=0)$ and $U-U(R_d=0)$ from perturbation method and from exact formulation, for various R_d and θ_R under the fixed Gr/Re value of 54. From the figures, it is observed that the perturbed solution is similar to the exact solution.

If both thermal radiation and rarefaction effects are considerable, the analytical solution of eqs. (18-23) can be expressed:

$$\begin{aligned}
&\theta+R_d(\theta+\theta_R)^4= \\
&=\left\{\begin{aligned}&\frac{-\theta_R}{c}+\frac{1}{c}\sqrt[3]{-\frac{c+\theta_R}{8cR_d}+\sqrt{\left(\frac{c+\theta_R}{8cR_d}\right)^2+\left(\frac{1}{3}-\frac{1}{12cR_d}\right)^3}}+\\&+\frac{1}{c}\sqrt[3]{-\frac{c+\theta_R}{8cR_d}-\sqrt{\left(\frac{c+\theta_R}{8cR_d}\right)^2+\left(\frac{1}{3}-\frac{1}{12cR_d}\right)^3}}\end{aligned}\right\}Y+ \\
&+1+(c-1)\left[\frac{-\theta_R}{c}+\frac{1}{c}\sqrt[3]{-\frac{c+\theta_R}{8cR_d}+\sqrt{\left(\frac{c+\theta_R}{8cR_d}\right)^2+\left(\frac{1}{3}-\frac{1}{12cR_d}\right)^3}}+\right. \\
&\left.+\frac{1}{c}\sqrt[3]{-\frac{c+\theta_R}{8cR_d}-\sqrt{\left(\frac{c+\theta_R}{8cR_d}\right)^2+\left(\frac{1}{3}-\frac{1}{12cR_d}\right)^3}}\right]+ \\
&+R_d\left[1+\sqrt[3]{-\frac{c+\theta_R}{8cR_d}+\sqrt{\left(\frac{c+\theta_R}{8cR_d}\right)^2+\left(\frac{1}{3}-\frac{1}{12cR_d}\right)^3}}+\right. \\
&\left.+\sqrt[3]{-\frac{c+\theta_R}{8cR_d}-\sqrt{\left(\frac{c+\theta_R}{8cR_d}\right)^2+\left(\frac{1}{3}-\frac{1}{12cR_d}\right)^3}}\right]^4
\end{aligned} \tag{45}$$

where $c=\lambda_T/2$. Equation (45) has a real solution only when the following condition is satisfied:

$$\theta_R>\frac{\sqrt{3}}{27}\left[\left(cR_d\right)^{-1/3}-4\left(cR_d\right)^{2/3}\right]^{3/2}-c \tag{46}$$

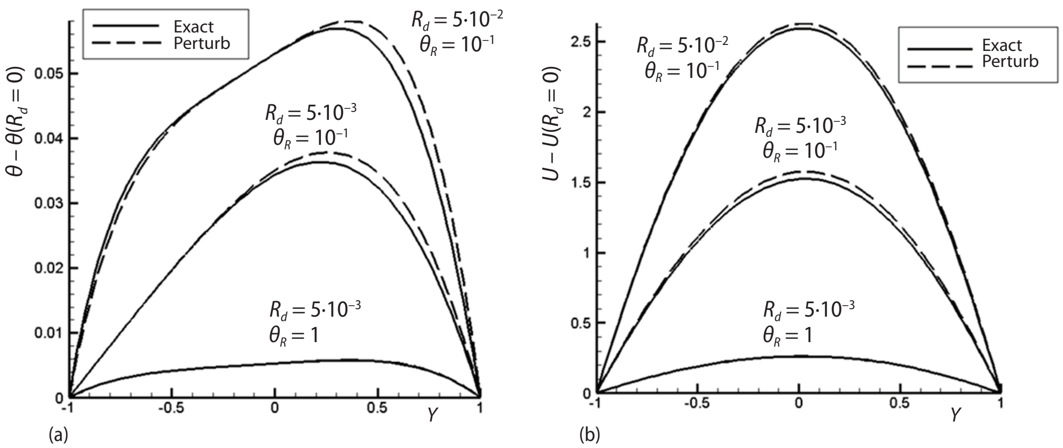

Figure 5. Comparison of $\theta - \theta(R_d = 0)$ and $U - U(R_d = 0)$ from perturbation method and from exact formulation, for various R_d and θ_R (Gr/Re = 54)

Therefore, if both R_d and θ_R are small, $\theta_R + c >\approx \sqrt{3}/27(cR_d)^{-1/2}$ and the flow in the channel could become unsteady. Equation (45) has the minimum as $-(4R_d)^{-1/3} - \theta_R$ and it should be less than zero to have a real solution. Therefore,

$$1 < \frac{3c^{1/3}}{4^{4/3}(cR_d)^{1/3}} + \sqrt[3]{-\frac{c+\theta_R}{8cR_d} + \sqrt{\left(\frac{c+\theta_R}{8cR_d}\right)^2 + \left(\frac{1}{3} - \frac{1}{12cR_d}\right)^3}} + \\ + \sqrt[3]{-\frac{c+\theta_R}{8cR_d} - \sqrt{\left(\frac{c+\theta_R}{8cR_d}\right)^2 + \left(\frac{1}{3} - \frac{1}{12cR_d}\right)^3}} \tag{47}$$

This inequality can identify the stable zone in ($\theta_R + \lambda_T/2$, $R_d\lambda_T$)-plane as illustrated in fig. 6. With decrease in c, the values of R_d and θ_R satisfying unsteady condition decreases.

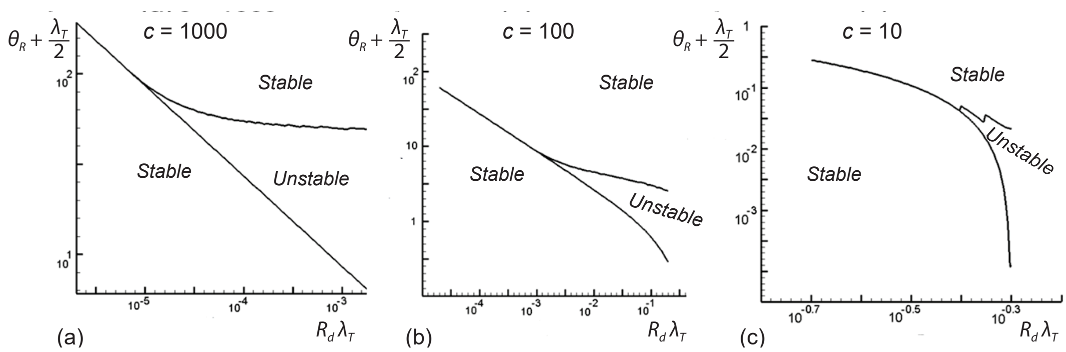

Figure 6. Stability diagrams in ($\theta_R + \lambda_T/2$, $R_d\lambda_T$)-plane for (a) c = 1000, (b) c = 100, and (c) c = 10

Conclusions and recommendation

In this study, the effect of thermal radiation on the steady flow in a vertical micro channel filled with highly absorbing medium has been thoroughly investigated. The results can be summarized as follows.

- When the thermal radiation is ignored, the behaviors of temperature and velocity are different: the temperature profile remains linear. At small Gr/Re, the velocity profile is parabolic while at large Gr/Re, it is changed as a sinusoidal shape.
- Grashof number, velocity slip, and pressure gradient increase skin friction and the Nusselt number whereas temperature jump and Reynolds number reduce their values.
- As R_d increases and θ_R decreases, the temperature profile becomes more non-linear.
- In the presence of thermal radiation, the maximum velocity increases with increase in θ_R. However, the velocity profile is not influenced by the thermal radiation.
- With inclusion of both thermal radiation and rarefaction effects, the values of R_d and θ_R satisfying unsteady condition decreases with decrease in c.

Acknowledgement

This work was supported by the Power Generation & Electricity Delivery Core Technology Program of the Korea Institute of Energy Technology Evaluation and Planning (KETEP), granted financial resource from the Ministry of Trade, Industry & Energy, Republic of Korea (No. 20131020102330).

References

[1] Barletta, A., Analysis of Combine Forced and Free Flow in a Vertical Channel with Viscous Dissipation and Isothermal-isoflux Boundary Conditions*, ASME J. Heat Transfer*, *121* (1999), 2, pp. 349-356
[2] Boulama, K., Galanis, N., Analytical Solution for Fully Developed Mixed Convection between Parallel Vertical Plates with Heat and Mass Transfer, *ASME J. Heat Transfer*, *126*, (2004), 3, pp. 381-388
[3] Hanafi, A. S., *et al.*,Thermal and Thydrodynamic Characteristics of Forced and Mixed Convection Flow Through Vertical Rectangular Channels, *Thermal Science*, *12* (2008), 2, pp. 103-117
[4] Babaelahi, M., *et al.*, Analytical Treatment of Mixed Convection Flow Past Vertical Flat Plate, *Thermal Science*, *14* (2010), 2, pp. 409-416
[5] Zhao, C. Y., Lu, T. J., Analysis of Microchannel Heat Sinks for Electronics Cooling, *Int. J. Heat Mass Transfer, 45*, (2002), 24, pp. 4857-4869
[6] Barletta, A., Fully Developed Mixed Convection and Flow Reversal in a Vertical Rectangular Duct with Uniform Wall Heat Flux, *Int. J. Heat Mass Transfer*, *45*, (2002), 3, pp.641-654
[7] Kandlikar, S. G., High flux Heat Removal with Microchannels – a Roadmap of Challenges and Opportunities, *Heat Transfer Eng*, *26* (2005), 8, pp. 5-14
[8] Hossain, M. S., *et al.*, Review on Solar Water Heater Collector and Thermal Energy Performance of Circulating Pipe, *Renew. Sust. Energy Rev.*, *15* (2011), 8, pp. 3801-3812
[9] Languri, E. M., *et al.*, An Energy and Exergy Study of a Solar Thermal Air Collector, *Thermal Science*, *13* (2009), 1, pp. 205-216
[10] Liu, D., Garimella, S. V., Investigation of Liquid Flow in Microchannels, *AIAA J. Thermophys. Heat Transfer, 18* (2004), 1, pp. 65-72
[11] Judy, J., *et al.*, Characterization of Frictional Pressure Drop for Liquid Flows through Microchannels, *Int. J. Heat Mass Transfer*, *45* (2002), 17, pp. 3477-3489
[12] Steinke, M. E., Kandlikar, S. G., Single-Phase Liquid Friction Factors in Microchannels, *Proceedings*, *2th ASME Conference on Microchannels and Minichannels*, Rochester, New York, USA, 2004
[13] Kandlikar, S. G., *et al.*, Characterization of Surface Roughness Effects on Pressure Drop in Microchannels, *Phys. Fluids*, *17* (2005), 10, ID100606
[14] Jamalabadi, M. Y. A. , *et al.*, Two-Dimensional Simulation of Thermal Loading with Horizontal Heat Sources, *Journal of Mechanical Engineering Science, 226* (2012), 5, pp. 1302-1308
[15] Jamalabadi, M. Y. A., *et al.*, Numerical Investigation of Thermal Radiation Effects on Open Cavity with Discrete Heat Sources, *Int. J. Numer Method Heat Fluid Flow, 23* (2013), 4, pp. 649-661
[16] Jamalabadi, M. Y. A., Experimental Investigation of Thermal Loading of a Horizontal Thin Plate Using Infrared Camera, *J. King Saud Univ. – Eng. Sci.*, *26* (2014), 2, pp. 159-167
[17] Jamalabadi, M. Y. A., Park, J. H., Thermal Radiation, Joule Heating, and Viscous Dissipation Effects on MHD Forced Convection Flow with Uniform Surface Temperature*, Open J. Fluid Dyn., 4* (2014), 2, pp. 125-132

[18] Uddin, Z., *et al.*, Influence of Thermal Radiation and Heat Generation/Absorption on MHD Heat Transfer Flow of a Micropolar Fluid Past a Wedge with Hall and Ion Slip Currents, *Thermal Science*, *18* (2014), 2, pp. 489-502

[19] Taylor, R. A., *et al.*, Nanofluid Optical Property Characterization: Towards Efficient Direct Absorption Solar Collectors, *Nanoscale Res. Lett.*, *6* (2011), 1, pp. 225-235

[20] Horvath, J. A., Webb, R. N., Experimental Study of Radiation Absorption by Microchannels of Varying Aspect Ratios, *Solar Energy*, *85* (2011), 5, pp. 1035-1040

[21] Hossain, M. S., *et al*., Review on Solar Water Heater Collector and Thermal Energy Performance of Circulating Pipe, *Renew. Sust. Energy Rev.*, *15* (2011), 8, pp. 3801-3812

[22] Crouch, J. D., *et al.*, Predicting the Onset of Flow Unsteadiness Based on Global Instability, *J. Comput. Phys.*, *224* (2007), 2, pp. 924-940

[23] Ulmanella, U., Ho, C. M., Molecular Effects on Boundary Condition in Micro/Nanoliquid Flows, *Phys. Fluids*, *20* (2008), 10, ID101512

[24] Bocquet, L., Barrat, J.-L., Flow Boundary Conditions From Nano- to Micro-Scales, *Soft Matter*, *3* (2007), 6, pp. 685-693

[25] Karniadakis, G., *et al*., *Microflows and Nanoflows: Fundamentals and Simulation*, Springer, New York, USA, 2005

[26] Modest, M. F., *Radiative Heat Transfer* (2nd ed.), Academic Press, New York, USA, 2003

Paper submitted: April 18, 2014
Paper revised: October 29, 2014
Paper accepted: November 2, 2014